Theory of Single Pion Production in Proton-Proton Collisions*†

J. IIZUKA‡ AND A. KLEIN
University of Pennsylvania, Philadelphia, Pennsylvania

(Received March 9, 1961)

Simple pion production in nucleon-nucleon collisions in the Bev energy region is studied by means of the picture due to Weiszäcker-Williams (peripheral interaction model) and in the $(\frac{3}{2},\frac{3}{2})$ resonance approximation for the final state pion-nucleon interaction. The excitation curve for the reaction $p+p \rightarrow p+n+\pi^+$, nucleon momentum distributions, and Q-value distributions in the center-of-mass system are calculated and compared with the published experimental data as well as with the work of Lindenbaum and Sternheimer. Agreement is reasonable with both, thus indicating that these particular distributions are insensitive to the isobar production mechanism (single pion exchange), though more recent experiments seem to have indicated clearly a preference for the theory developed here.

I. INTRODUCTION

PION production in nucleon-nucleon collisions is one of the most familiar phenomena in the Bev energy region. Thus a number of works[1] have been published attacking this problem from a variety of aspects. In particular, Belenki and Nikishov[2] and Lindenbaum and Sternheimer[3] have extensively analyzed the single and the double production in nucleon-nucleon collisions by means of the isobar model and they have found good agreement between their results and the experimental data.

From a completely theoretical viewpoint, Henley and Lee[4] have proposed an approach based on the intermediate coupling meson theory and the Lewis, Oppenheimer, and Wouthuysen theory[5] of multiple pion production in the cosmic-ray energy region.

More recently the conviction has grown that the Weiszäcker-Williams picture or the peripheral interaction model may well describe the Bev pion phenomena. In fact, Kobayashi[6] has studied the excitation curve of the reaction $p+p \rightarrow p+n+\pi^+$ and has obtained reasonable agreement with the experimental data of Fowler *et al.*[7] Quite recently Selleri[8] has also produced striking evidence in favor of this model by studying the neutron kinetic energy spectrum of the above reaction in the laboratory system.

In these circumstances, we consider it worthwhile to re-examine the implications of the $(\frac{3}{2},\frac{3}{2})$ resonance model as modified by the peripheral interaction idea, and in particular to compare the results both with experiment and with the more schematic model of Lindenbaum and Sternheimer. Toward this end we shall study the aforementioned reaction in the c.m. system and calculate the nucleon momentum distribution, the Q-value distribution, the neutron recoil distribution, and the cross section.

In our treatment of the problem the following approximations will be made:

(i) One pion exchange process between nucleons is mainly responsible for the phenomenon.

(ii) The virtual scattering amplitude, which appears in this problem, is dominantly large in the $(\frac{3}{2},\frac{3}{2})$ state of the c.m. pion-nucleon system.

(iii) The $(\frac{3}{2},\frac{3}{2})$ virtual scattering amplitude is well approximated by the corresponding energy shell amplitude.

We shall give the kinematical considerations and the analytic formulas for the observable quantities in Sec. II. In Sec. III we shall give our numerical calculations and comparison with the experimental results as well as with previous theoretical work. Finally the last section is given over to a summary and conclusions.

II. OUTLINE OF THE THEORY

Let us take the 4-momenta of the initial nucleons to be p_1 and p_2, and those of the final nucleons and of the pion to be p_1', p_2', and q, respectively, (see Fig. 1). The

* Supported in part by the U. S. Atomic Energy Commission.

† *Note added in proof.* Owing to an error in the normalization of the initial state vector, the total cross section given in Eq. (8) and plotted in Fig. 2 should each be multiplied by a factor of 2, thus destroying the quantitative agreement with experiment. The remaining results of the paper which involve only comparison of shapes are unchanged. Neither the previous agreement nor the present disagreement can be said to be well understood in view of the many approximations made. We are indebted to Dr. G. C. Wick and Dr. F. Salzman for pointing out the error to us, which appears also to have been made in the works of Kobayashi and Seleri referred to in the text.

‡ Present address: Enrico Fermi Institute for Nuclear Studies, University of Chicago, Chicago, Illinois.

[1] For the kinematical analysis, see A. H. Rosenfeld, Phys. Rev. **96**, 139 (1954); M. Gell-Mann and K. M. Watson, Ann. Rev. Nuclear Sci. **4**, 219, (1954); D. Ito and S. Minani, Progr. Theoret. Phys. (Kyoto) **14**, 108 (1954); D. Ito, S. Minani, and H. Tanaka, Nuovo cimento **8**, 135; and **9**, 208 (1958). For the isobar model, see D. C. Peaslee, Phys. Rev. **94**, 1085; and **95**, 1580 (1954); J. S. Kovacs, *ibid.* **101**, 397 (1956); S. Barshay, *ibid.* **106**, 572 (1957); S. Mandelstam, Proc. Roy. Soc. (London) **A244**, 492 (1958).

[2] S. Z. Belenki and A. I. Nikishov, Soviet Phys.—JETP **1**, 593 (1955).

[3] S. J. Lindenbaum and R. M. Sternheimer, Phys. Rev. **105**, 1874 (1957).

[4] E. M. Henley and T. D. Lee, Phys. Rev. **101**, 1536 (1956).

[5] H. V. Lewis, J. R. Oppenheimer, and A. S. Wouthuysen, Phys. Rev. **73**, 127 (1948).

[6] T. Kobayashi, Progr. Theoret. Phys. (Kyoto) **18**, 318 (L) (1957).

[7] W. B. Fowler *et al.*, Phys. Rev. **103**, 1476, 1484, and 1489 (1956).

[8] F. Selleri, Phys. Rev. Letters **6**, 64 (1960). Selleri's basic approach is essentially the same as ours. We are indebted to Professor Y. Nambu for showing us a prepublication copy of Selleri's work.

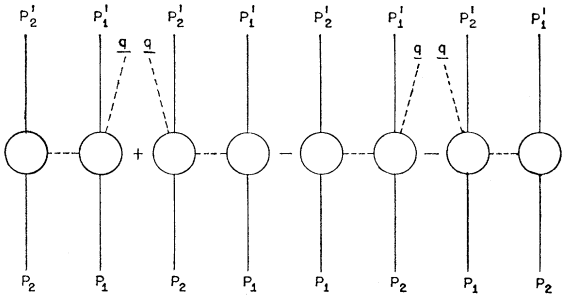

FIG. 1. The diagrammatical representation of $T_{(1)}$.

S matrix for the process is given as follows:

$$\langle(-)p_1'p_2'q_\beta|p_1p_2(+)\rangle = -(2\pi)^4\delta^4(p_1'+p_2'+q-p_1-p_2)\times\left[\frac{M^4}{2q_0p_{10}'p_{20}'p_{10}p_{20}}\right]^{\frac{1}{2}}T_{fi},$$

$$T_{fi}=\sum_{n=1}^{\infty}T_{(n)},$$

$$T_{(1)}=\left[\frac{2q_0p_{10}'p_{20}'p_{10}p_{20}}{M^4}\right]^{\frac{1}{2}}\times\{\langle(-)p_1'q|j(0)|p_1\rangle(\Delta_F(p_2-p_2'))^2\times\Delta_F'^{-1}(p_2-p_2')\langle p_2'|j(0)|p_2\rangle+\langle(-)p_2'q|j(0)|p_2\rangle(\Delta_F(p_1-p_1')^2\Delta_F'^{-1}(p_1-p_1')\times\langle p_1'|j(0)|p_1\rangle-(\text{the same expression with } p_1\leftrightarrow p_2)\},\quad(1)$$

where $T_{(n)}$ with $n\geq 2$ denotes the contribution to T_{fi} from the n-pion exchange process between nucleons. $|n(-)\rangle$ is the incoming state with character n and we have omitted the isospin index in the above equations. $j(0)$ is defined by the Heisenberg equation for the pion field,

$$(\Box-\mu^2)\phi(x)=j(x).\quad(2)$$

The above expression for the T matrix can be obtained from the extension of the method due to Klein and McCormick[9] in the nuclear force problem.

The virtual pion-nucleon scattering[10] and the vertex parts in Eq. (1) can be shown to have the form

$$H_{\beta\alpha}=\langle(-)p_i'q_\beta|j_\alpha(0)|p_j\rangle(2q_0p_{i0}'p_{j0}/M^2)^{\frac{1}{2}}=K(t^2)\bar{u}(p_i')[A(\nu,\nu_B,t^2)+i\gamma\cdot qB(\nu,\nu_B,t^2)]u(p_j),\quad(3)$$

$$\langle p_i'|j_\alpha(0)|p_j\rangle(p_{i0}'p_{j0}/M^2)^{\frac{1}{2}}=K(t^2)\bar{u}(p_i')ig\gamma_5\tau_\alpha u(p_j),$$

where α and β denote the isospin indices and $A(\nu,\nu_B,t^2)$ and $B(\nu,\nu_B,t^2)$ are the now familiar invariant functions for pion-nucleon scattering.[11] The invariant parameters ν, ν_B, and t^2 are defined as follows:

$$\nu=-\frac{1}{2M}q\cdot(p_i'+p_j),\quad \nu_\beta=\frac{q\cdot t}{2M},\qquad t^2=(p_i'+q-p_j)^2.\quad(4a)$$

$K(t^2)$ was introduced by Federbush *et al.*[12] and is related to the vertex function $\Gamma_5(t^2)$ by the equation

$$K(t^2)=\Delta_F^{-1}(t^2)\Delta_F'(t^2)\Gamma_5(t^2).\quad(4b)$$

We next define the partial wave amplitudes $f_{l\pm}^T$ as follows:

$$-\frac{M}{4\pi W}\bar{u}(p_i')[A+i\gamma\cdot qB]u(p_j)=\sum_{l,T}(2l+1)\{P_{Jl}^{(+)}(x)f_{l+}^T(W,t^2)+P_{Jl}^{(-)}(x)f_{l-}^T(W,t^2)\},\quad(5)$$

$$x=\hat{q}\cdot\hat{t}=(2M\nu_B+q_0t_0)/qt,$$

where q_0, t_0, q, and t are the energies and the momenta of the final and of the virtual pion in the c.m. final pion-nucleon system with the total energy $W(p_i'$ and $q)$. $P_{Jl}^{(\pm)}(x)$ is the eigenfunction of the total angular momentum $J=l\pm\frac{1}{2}$. T means the total isospin of the pion-nucleon system. In the $(\frac{3}{2},\frac{3}{2})$ resonance model, we take

$$-(M/4\pi W)\bar{u}(p_i')[A+i\gamma\cdot qB]u(p_j)\approx 3f_{1+}^{\frac{3}{2}}(W,t^2)P_{\frac{3}{2},1}^{(+)}(x),\quad f_{1+}^{\frac{3}{2}}(W,t^2)=p(\tfrac{3}{2})f_{3,3}(W,t^2),\quad P_{\frac{3}{2},1}^{(+)}(x)=x-\tfrac{1}{3}\boldsymbol{\sigma}\cdot\hat{q}\boldsymbol{\sigma}\cdot\hat{t},\quad(6)$$

where $p(\frac{3}{2})$ is the projection operator for $T=\frac{3}{2}$, and $\hat{q}\equiv\mathbf{q}/|\mathbf{q}|$. Furthermore, the energy shell approximation means that

$$f_{3,3}(W,t^2)\approx\frac{e^{i\delta_{33}}}{q}\sin\delta_{33},\quad(7)$$

where δ_{33} is the phase of the real pion-nucleon scattering at the c.m. system total energy W. Other possible approximations for $f_{3,3}(W,t^2)$ will be discussed in Sec. IV.

Now let us consider more specifically the cross section for the reaction $p+p\rightarrow p+n+\pi^+$. In the peripheral interaction model with the $(\frac{3}{2},\frac{3}{2})$ resonance

[9] A. Klein and B. H. McCormick, Phys. Rev. **104**, 1749 (1956). For details see J. Iizuka, Ph.D. thesis, University of Pennsylvania, 1961 (unpublished).

[10] S. Fubini, Y. Nambu, and V. Wataghin, Phys. Rev. **111**, 329 (1958); J. Iizuka and A. Klein, Progr. Theoret. Phys. (to be published).

[11] G. F. Chew, M. L. Goldberger, F. E. Low, and Y. Nambu, Phys. Rev. **106**, 1337 (1957).

[12] P. Federbush, M. L. Goldberger, and S. B. Treiman, Phys. Rev. **112**, 642 (1958).

and the energy shell approximations, we have[13]

$$\sigma=(2\pi)^4\tfrac{1}{4}\sum_{\text{spin } i,f}\frac{M^2}{2B_0}\times\int\delta^4(p_1'+p_2'+q-p_1-p_2)\,|\,T_{(1)}\,|^2 dJ, \quad (8)$$

where

$$B^0=[(\mathbf{p}_1p_{20}-\mathbf{p}_2p_{10})^2-(\mathbf{p}_1\times\mathbf{p}_2)^2]^{\frac{1}{2}},$$

$$dJ=\frac{M}{(2\pi)^3}\frac{d^3p_1'}{p_{10}'}\frac{M}{(2\pi)^3}\frac{d^3p_2'}{p_{20}'}\frac{1}{(2\pi)^3}\frac{d^3q}{2q_0}.$$

The spin average and sum in the initial and the final state is indicated by $\frac{1}{4}\sum_{\text{spin } i,f}$ and the factor $\frac{1}{2}$ comes from the initial flux normalization.

We may write Eq. (8) as follows:

$$\sigma=\frac{20}{9}\sigma(a)+\frac{10}{9}\sigma(b)-\frac{2}{3}\sigma(c), \quad (9)$$

where $\sigma(a)$ is given by Eq. (8) with the replacement of $T_{(1)}$ by its first term as given in Eq. (1), in which p_1' and p_2' refer to the proton and the neutron state, respectively. $\sigma(b)$ comes from the interference between the first and the third term, while $\sigma(c)$ comes from the interference between the first and the fourth term. The coefficients of $\sigma(i)$ in Eq. (9) can be easily understood if we remark that in $\sigma(i)$, the matrix element corresponding to the virtual-pion nucleon scattering part is always taken as that of π^+p scattering. For reference, we shall give the relations similar to Eq. (9) for the other reactions:

$$\begin{aligned}
\sigma(p+p\to p+p+\pi^0)&=\frac{4}{9}\sigma(a)+\frac{2}{9}\sigma(b)+\frac{2}{9}\sigma(c),\\
\sigma(p+n\to p+n+\pi^0)&=\frac{8}{9}\sigma(a)+\frac{4}{9}\sigma(b)-\frac{4}{9}\sigma(c),\\
\sigma(p+n\to p+p+\pi^-)&=\frac{2}{9}\sigma(a)+\frac{1}{9}\sigma(b)+\frac{2}{9}\sigma(c),\\
&=\sigma(p+n\to n+n+\pi^+).
\end{aligned} \quad (10)$$

Before going into the details of the evaluation of the $\sigma(i)$, we discuss the branching ratios predicted by the $(\frac{3}{2},\frac{3}{2})$ resonance model. The familiar branching ratios do not naturally follow from Eqs. (9) and (10) because of the existence of the interference term $\sigma(c)$. But, as discussed by Henley and Lee,[4] in order that $\sigma(c)$ be large, two final nucleons must emerge essentially in the same direction with the same energy (see Fig. 1), which is an unlikely event. Physically speaking this also means that the wave function of the final nucleon p_2' with and without scattering between itself and pion q may not have the same phase, and as a consequence $\sigma(c)$ may be expected to be quite small. Thus if we neglect this term, we reach the branching ratios of the isobar model, i.e.,

$$\begin{aligned}
&\sigma(p+p\to p+n+\pi^+)/\sigma(p+p\to p+p+\pi^0)=5,\\
&\sigma(p+p\to p+n+\pi^+)/\sigma(p+n\to p+p+\pi^-)=10.
\end{aligned} \quad (11)$$

We shall adhere to this approximation throughout the remainder of this work.

We next turn to a detailed discussion[14] of the $\sigma(i)$. We have in the center of mass of the initial system,

$$\sigma(a)=\frac{1}{(2\pi)^3}\frac{g^2}{2p_cW_c}\int\delta^4(p_1'+p_2'+q-p_1-p_2)dj\times\frac{t^2}{(t^2+1)^2}\left(\frac{W}{q}\right)^2\sin^2\delta_{33}(3x^2+1),$$

$$\sigma(b)=-\frac{1}{(2\pi)^3}\frac{g^2}{2p_cW_c}\int\delta^4(p_1'+p_2'+q-p_1-p_2)dj\times\frac{1}{(t^2+1)(t_e^2+1)}\left(\frac{W}{q}\right)^2\sin^2\delta_{33}\times\frac{\mathfrak{M}}{[(E_{1s}+M)(E_{2s}+M)]^{\frac{1}{2}}}, \quad (12)$$

$$\mathfrak{M}=\tfrac{1}{4}(W+M)(\mathbf{p}_{1s}\cdot\mathbf{p}_{2s})xx_e+\tfrac{1}{12}(W+M)p_{1s}p_{2s}(x^2+x_e^2)+(\tfrac{1}{12}xx_e-\tfrac{1}{36}(\hat{p}_{1s}\cdot\hat{p}_{2s}))(W-M)(E_{1s}+M)\times(E_{2s}+M)-\tfrac{1}{36}(W+M)p_{1s}p_{2s},$$

where the following notation is used:

$$dj=\frac{d^3p_1'}{p_{10}'}\frac{d^3p_2'}{p_{20}'}\frac{d^3q}{q_0},$$

$$t=p_1'+q-p_1=p_2-p_2',\quad t_e=p_1-p_2',$$

$$x=\hat{q}\cdot\hat{t},\quad x_e=\hat{q}\cdot\hat{t}_e,$$

and p_{is} and E_{is} are the momentum and the energy of the initial nucleon i in the c.m. system of p_1' and q. p_c and W_c are the momentum of the initial nucleon and the total energy of the initial system in its own c.m. system.

The integration[15] of Eq. (12) can be carried out for

[13] C. Møller, Kgl. Danske Videnskab. Selskab, Mat-fys. Medd. **23**, 1 (1945).

[14] In the following we shall neglect the correction coming from the vertex and pion propagator modification, i.e.,

$$\Gamma_5(t^2)\Delta_F^{-1}(t^2)\Delta_F'(t^2)\Gamma_5(t^2)=1.$$

[15] Formulas equivalent to Eq. (13) have been worked out by F. Selleri, reference 8. For details, see reference 9.

the variables p_1' and q;

$$\frac{d\sigma(a,p_{20}')}{dp_{20}'}=\frac{g^2}{2\pi}\frac{1}{p_cW_c}\left(\frac{W}{q}\right)\sin^2\delta_{33}(W)\times\left[\frac{1}{p_c}\ln\left(\frac{W_cp_{20}'-2M^2+1+2p_cp_2'}{W_cp_{20}'-2M^2+1-2p_cp_2'}\right)-\frac{4p_2'}{(W_cp_{20}'-2M^2+1)^2-4p_c^2p_2'^2}\right],$$

$$\frac{d\sigma(b,p_{20}')}{dp_{20}'}=\frac{g^2}{2\pi^2}\frac{1}{4p_cW_c}\left(\frac{W}{q}\right)\sin^2\delta_{33}(W)\int d\Omega_{p_2'p_2'}\times\frac{1}{(t^2+1)(t_e^2+1)}\frac{1}{[(E_{1s}+M)(E_{2s}+M)]^{\frac{1}{2}}}\times\{(W-M)(E_{1s}+M)(E_{2s}+M)(\hat{p}_{1s}\cdot\hat{p}_{2s})+\tfrac{1}{2}(W+M)p_{1s}p_{2s}[3(\hat{p}_{1s}\cdot\hat{p}_{2s})^2-1)\}. \tag{13}$$

In the integrals the range of p_{20}' is

$$[M,\ (W_c^2-2M-1)/2W_c].$$

Momentum and Q-value distributions are obtained from Eqs. (12) and (13) with the help of elementary isospin considerations. Here we shall give only the results:

(i) The proton momentum distribution and the Q-value distribution of the neutron-pion pair are (see below for definitions)

$$\frac{d\sigma(p_1')}{dp_1'}=\frac{p_1'}{p_{10}'}\left[\frac{2}{9}\frac{d\sigma(a,p_{10}')}{dp_{10}'}+\frac{1}{9}\frac{d\sigma(b,p_{10}')}{dp_{10}'}+2\frac{d\sigma(\tilde{a},p_{10}')}{dp_{10}'}+\frac{d\sigma(\tilde{b},p_{10}')}{dp_{10}'}\right], \tag{14}$$

$$\frac{d\sigma(Q_{n\pi^+})}{dQ_{n\pi^+}}=\frac{W}{W_c}\{\text{the above expression}\}, \tag{15}$$

$$Q_{n\pi^+}=W-M-1.$$

(ii) The neutron momentum distribution and the Q-value distribution of the proton-pion pair are

$$\frac{d\sigma(p_2')}{dp_2'}=\frac{p_2'}{p_{20}'}\left\{2\frac{d\sigma(a,p_{20}')}{dp_{20}'}+\frac{d\sigma(b,p_{20}')}{dp_{20}'}+\frac{2}{9}\frac{d\sigma(\tilde{a},p_{20}')}{dp_{20}'}+\frac{1}{9}\frac{d\sigma(\tilde{b},p_{20}')}{dp_{20}'}\right\}, \tag{16}$$

$$\frac{d\sigma(Q_{p\pi^+})}{dQ_{p\pi^+}}=\frac{W}{W_c}\{\text{the above expression}\}. \tag{17}$$

In Eqs. (14) to (17), $d\sigma(\tilde{a},p_{i0}')/dp_{i0}'$ or $d\sigma(\tilde{b},p_{i0}')/dp_{i0}'$ mean that these quantities are calculated from Eq. (12) by a change of the order of integration, i.e., by interchanging the roles of the two final nucleons; for example, to calculate the contribution to the proton momentum distribution from the first term of $T_{(1)}$, the p_2' and q integrations must be carried out first. This order of integrations is quite complex and we have used the following approximate form for $\sigma(a)$ which will be justified in the Appendix:

$$\frac{d\sigma(\tilde{a},p_{i0}')}{dp_{i0}'}\approx\frac{g^2}{2\pi}\frac{1}{p_cW_c}\int_{E-}^{E+}dp_{j0}'\frac{p_i'}{p_c}\left(\frac{W'}{q'}\right)^2\sin^2\delta_{33}(W')\times\left[\frac{1}{6}\ln\left(\frac{p_i'a+p_cb}{p_i'a-p_cb}\right)-\frac{2p_i'p_c}{(p_i'a)^2-(p_cb)^2}\right], \tag{18}$$

where

$$a=W_cp_{j0}'+1-2M^2,$$
$$b=W^2+M^2-1-2p_{j0}'(W_c-p_{i0}'),$$
$$W^2=W_c^2+M^2-2W_cp_{i0}',\quad W'^2=W_c^2+M^2-2W_cp_{j0}',$$
$$q'^2=[(W'+M)^2-1][(W'-M)^2-1]/4W'^2,$$
$$E_\pm=\{(W_c-p_{i0}')(W^2+M^2-1)\pm p_i'[(W^2+M^2-1)(W^2-3M^2-1)]^{\frac{1}{2}}\}/2W^2.$$

Although we could not obtain any simple expression for $d\sigma(\tilde{b},p_{i0}')/dp_{i0}'$, we shall see in the next section that this interference term is quite small. Thus we shall neglect $d\sigma(\tilde{b},p_{i0}')/dp_{i0}'$ in the discussion of the momentum and of the Q-value distributions.

(iii) In the same way, we have for the neutron recoil spectrum

$$\frac{d\sigma(p_2'\Omega_2)}{dp_2'd\Omega_2}\approx\frac{g^2}{2\pi^2}\frac{1}{p_cW_c}\frac{p_2'^2}{p_{20}'}\left(\frac{W}{q}\right)\sin^2\delta_{33}\times\left[\frac{t^2}{(t^2+1)^2}+\frac{t_e^2}{(t_e^2+1)^2}\right]+\frac{d\sigma(b,\Omega_2)}{dp_2'd\Omega_2}+\frac{1}{9}\left[\frac{d\sigma(\tilde{a},p_2',\Omega_2)}{dp_2'd\Omega_2}+\frac{d\sigma(\tilde{a},p_2',\Omega_2)}{dp_2'd\Omega_2}\right]+\frac{1}{9}\frac{d\sigma(\tilde{b},p_2',\Omega_2)}{dp_2'd\Omega_2}. \tag{19}$$

The interpretation of Eq. (19) will be clear from the above discussion. In the actual computation of the neutron recoil spectrum we have dropped the last two terms, whose contributions are again expected to be quite small (see next section).

Now, at this stage, we shall compare our expressions with those of Lindenbaum and Sternheimer. As is well known, the Lindenbaum-Sternheimer picture for the production mechanism consists of the following three points: (i) An isobar can be treated as a real unstable particle. (ii) The isobar production rate is proportional to the phase volume of the isobar-nucleon system and to the total cross section of the $\pi^\pm p$ system. (iii) Angular distributions for the formation and decay of the isobar are arranged so as to fit the experimental data. Thus they have combined the features of Fermi's statistical model and the fact of the strong $(\frac{3}{2},\frac{3}{2})$ pion-nucleon

interaction. Because of this combined viewpoint, they were forced to make various assumptions. In particular their angular momentum considerations are quite ambiguous. On the other hand, in our treatment the one-pion-exchange approximation completely eliminates a series of assumptions made by them.

From the above comparison, we may expect that differences between our results and those of Lindenbaum-Sternheimer will appear in the quantities including strong angular dependences like the neutron recoil spectrum.

III. NUMERICAL CALCULATIONS AND DISCUSSION

Before going into the details of the numerical calculations, we shall make a remark concerning the pion-nucleon scattering part, $\sin^2\delta_{33}/q^2$. For this quantity we have taken experimental data[16] and for the sake of comparison have also used the Chew-Low formula[17] which has the form

$$\frac{\sin^2\delta_{33}}{q^3} \simeq \frac{(\omega_r/q_0)^2\lambda^2 q^3}{(q_0-\omega_r)^2+(\omega_r/q_0)^2\lambda^2 q^6}, \tag{20}$$

where $\omega_r(=1.91)$ is the pion energy at the $(\frac{3}{2},\frac{3}{2})$ resonance and $\lambda^2=(\frac{4}{3}f^2)^2$, $f^2=0.08$.

Numerical calculations were made with a desk computer by means of Simpson's formula, with the range of integration for p_{i0}', $[M, (Wc^2-2M^2-1)/2Wc]$, divided into ten intervals for each case.

A. Energy Dependence of the Cross Section for the Reaction $p+p\rightarrow p+n+\pi^+$

Figure 2 compares the theoretical and the experimental results.[18] Our curves (a) and (b) are obtained

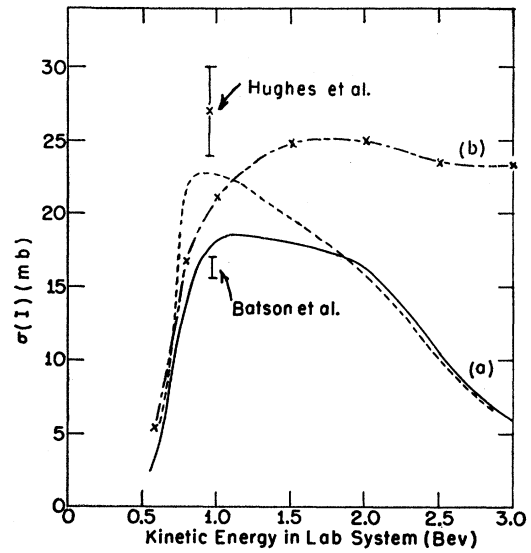

FIG. 2. The excitation curve for the reaction $p+p\rightarrow p+n+\pi^+$.

[16] H. L. Anderson, W. C. Davidson, and U. E. Kruse, Phys. Rev. **100**, 339 (1955).
[17] G. F. Chew and F. E. Low, Phys. Rev. **101**, 1570 (1956).
[18] See reference 7.

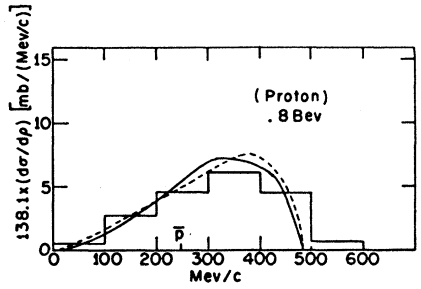

FIG. 3. Proton momentum distribution at 0.8 Bev. In Figs. 3–18, histograms give the experimental values; where they occur, the dashed curves refer to the theory of Lindenbaum and Sternheimer, the solid curves to the present theory.

by the substitution of experimental data and the Chew-Low formula, Eq. (20), for the pion-nucleon scattering part, respectively. The curve (a) is quite similar to that obtained by Kobayashi.[6] In Eq. (9), the contribution $\sigma(b)$, which is the interference term between the first and third diagrams of Fig. (1), decreases from about a fourth at 0.6 Bev to about a twelfth of $\sigma(a)$ at 3 Bev. Considering the factor coming from isospin considerations in Eq. (9), the term $\sigma(b)$ does not therefore contribute significantly to the reaction $p+p\rightarrow p+n+\pi^+$. This is the reason for agreement between our curve (a) and that of Kobayashi, who did not include this term.

The experimental data in the region 0.8 to 1.2 Bev are not all consistent, as we see from Fig. 2. This also seems to be true for the momentum distribution of the proton. Thus it is difficult to say whether or not the theoretical results "agree" with the experimental data in this energy region. If the work of Hughes *et al.*[19] turned out to be correct, the interpretation of the extra 9 mb would be an important problem. On the other hand, our curve slightly exceeds the result of Batson *et al.*[20] For the tail of the excitation curve, we have reasonable agreement, although the theoretical values seem to exceed the experimental one at around 1.7 Bev. This tendency has also appeared in the work of Kobayashi.[21] The most probable reason for the largeness

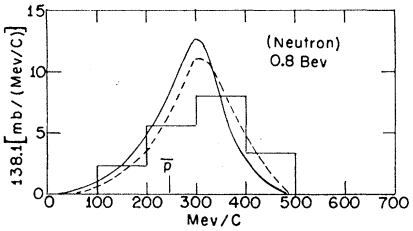

FIG. 4. Neutron momentum distribution at 0.8 Bev.

[19] I. S. Hughes *et al.*, Phil. Mag. **2**, 215 (1957).
[20] A. P. Batson *et al.*, Proc. Roy. Soc. (London) **A251**, 218 (1959).
[21] According to Kobayashi's work, this critical energy is about 1.4 Bev. This difference might be based on different analytic formula for σ, i.e., because of the different approximation.

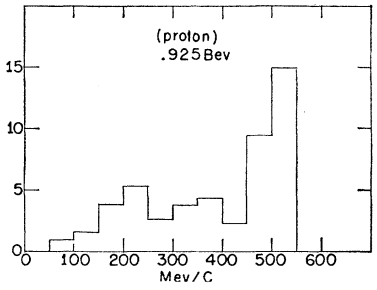

FIG. 5. Proton momentum distribution at 0.925 Bev.

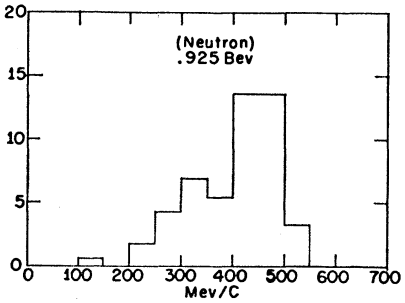

FIG. 6. Neutron momentum distribution at 0.925 Bev.

of the theoretical curve is the inadequacy of the energy shell approximation, i.e., if the virtual pion is far off the energy shell ($t^2>$ a few M), $f_{3,3}(W,t^2)$ cannot be reasonably equated with the energy shell amplitude, Eq. (7). The curve (b) in Fig. 2 shows the result of adopting the Chew-Low formula, Eq. (10), for $\sin^2\delta_{33}/q^2$. This does not give any damping feature up to 3 Bev, although the cross section is expected to decrease faster than $(1/W_c^2)\ln W_c$ at high energies. This result may not be surprising, because the Chew-Low formula would be only appropriate in the low-energy region [at most up to the $(\frac{3}{2},\frac{3}{2})$ resonance energy].

B. Momentum and Kinetic Energy Distributions of the Nucleon

Figures 3 to 12 show the momentum and the kinetic energy distributions of the nucleons. Our theoretical curves (solid lines) as well as the experimental ones (histograms) are normalized so as to give 138.1 times the theoretical cross section at each energy, when integrated over the momentum which forms the abscissa.

We first remark that our curves are quite similar to those (dashed lines) obtained by Lindenbaum and Sternheimer. However, for the proton distribution at 0.8 Bev the maximum is appreciably shifted[22] (about 90 Mev/c). The similarity among these curves means that the matrix elements, except for the pion-nucleon scattering part, do not differ significantly compared to the product of phase volume and Lorentz transformation factor taken by the above authors.

Secondly the sharp maximum in the neutron distribution, compared to the proton case, is a characteristic feature of the isobar model, as we easily see from Eqs. (13) and (16). In this respect we notice that $d\sigma(a,p)/dp$ strongly reflects the shape of the pion-nucleon scattering cross section; on the other hand, $d\sigma(\tilde{a},p)/dp$ behaves more or less like the phase volume below 1.5 Bev with a broad maximum at a value at about half that of $d\sigma(a,p)/dp$. $d\sigma(b,p)/dp$ has a shape similar to $d\sigma(a,p)/dp$, but is in magnitude at most less than one-tenth of the latter beyond 0.8 Bev. $d\sigma(\tilde{b},p)/dp$ is expected to have the same behavior as that of $d\sigma(\tilde{a},p)/dp$. Considering these facts, we can approximate the momentum distribution well by neglecting $d\sigma(\tilde{b},p)/dp$. This term can only contribute a few percent to the flat background of the distributions (actually $d\sigma(\tilde{b},p)/dp$ as well as $d\sigma(b,p)/dp$ yield negative values).

Now the values of the momentum, $\bar{p}$, of the nucleon at the maxima of the curves are determined by the relation

$$\bar{p}=[(W_c+M)^2-\bar{W}]^{\frac{1}{2}}[(W_c-M)^2-\bar{W}^2]^{\frac{1}{2}}/2W_c, \quad (21)$$

where $\bar{W}$ is the total energy of the pion-nucleon scattering at resonance. The failure of the above relation at 0.8 Bev comes from the destructive interference between the pion-nucleon scattering part and the rest of the matrix element.

Next let us turn to the comparison with experimental data. The histograms shown in Figs. 3, 4, 11, and 12 are quoted from the works of Fowler *et al.*,[7] while in Figs. 7 to 10 works of Batson *et al.*[20] (0.97 Bev) are quoted. In particular the histograms of Figs. 7 and 8 are calculated from the energy spectra given by Batson *et al.* by assuming that the transformation factor p/p_0 between the two distributions is approximated by the

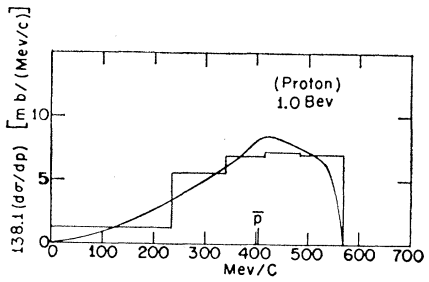

FIG. 7. Proton momentum distribution at 1.0 Bev.

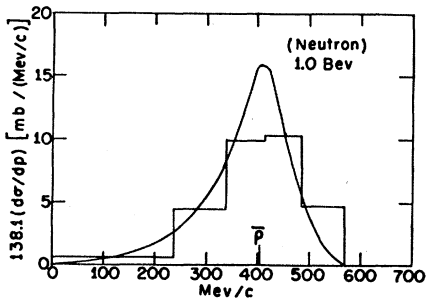

FIG. 8. Neutron momentum distribution at 1.0 Bev.

[22] See the discussion of the recoil neutron spectrum in the later section.

ratio $\Delta p_0/\Delta p$ for each interval in Figs. 7 to 10. We have made this transformation for the sake of comparison with the works of Hughes *et al.*[19] at 0.925±0.030 Bev, Figs. 5 and 6.

As discussed by Lindenbaum and Sternheimer, the theoretical curves are in good agreement with the experimental data at 0.8 and 1.5 Bev, if we keep in mind that the experimental data is rather crude at these energies. At about 1.0 Bev, the experimental information is rather poor. Although Figs. 7 to 10 show good agreement, this may not be taken seriously, as we see from Figs. 5 and 6. In particular, the proton momentum distribution seems to show the possible existence of a peak at around 200 Mev/c (Figs. 5 and 6). Although this experiment has been done at proton energy 925±30 Mev, it would be surprising if the 50-Mev difference between this and the neighboring experiment at 970 Mev gives this marked difference in the proton distributions. To give a proton momentum distribution similar to Fig. 5 at 970 Mev it would be necessary that the kinetic energy distribution have a rather sharp peak at around 28 Mev and a minimum at around 60 Mev. But Fig. 9 seems to show no such tendency. The discrepancies in the experimental data at this energy were also mentioned in connection with the excitation curve of the reaction $p+p \rightarrow p+n+\pi^+$.

C. Q-Value Distribution of the Pion-Nucleon Pairs

The discussion of the Q-value distributions can be carried out in parallel with that of the nucleon momentum distributions. Figs. 13 to 18 show the Q-value distributions for the nucleon-pion pairs, the normalizations in these figures being the same as those of the momentum distribution cases. The histograms in the figures are quoted from the works mentioned in the momentum distribution case.

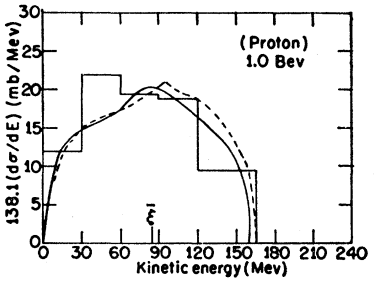

FIG. 9. Proton kinetic energy distribution at 1.0 Bev.

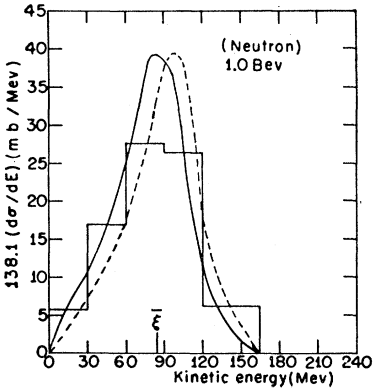

FIG. 10. Neutron kinetic energy distribution at 1.0 Bev.

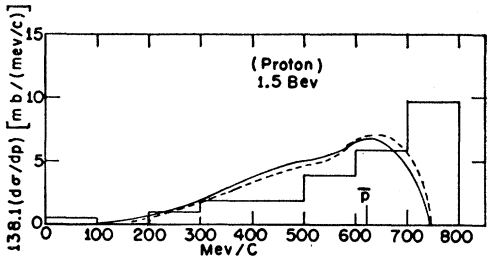

FIG. 11. Proton momentum distribution at 1.5 Bev.

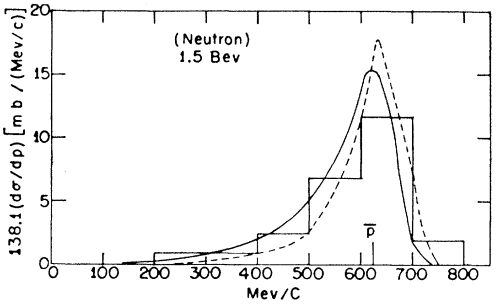

FIG. 12. Neutron momentum distribution at 1.5 Bev.

Again our curves (solid lines) are similar to those (dashed lines) of Lindenbaum and Sternheimer, though slight differences are observed for the $n\pi^+$-pair at 0.8 and 1.5 Bev.

As the counterpart of the neutron momentum distribution, we have sharp distributions for the $p\pi^+$-pair and the values of Q, $\bar{Q}$, at the maxima of the curves are given by $\bar{Q}=\overline{W}-M-1$, with the exception of the 0.8-Bev case. Although the agreement between the theoretical curves and the experimental results seems to be bad at 0.8 and 1.5 Bev, whether or not this disagreement is serious would be determined by much more accurate experimental data, because at 1.0 Bev the agreement is very good and we believe this is not the accidental one.

D. Recoil Nucleon Spectrum

For these quantities, we have only studied the neutron case at 1.0 Bev. Although we have no experimental data with which to compare, we have included this spectrum for the following reason. As we see from Eq. (19), only this quantity seems to emphasize the main distinguishing feature of the peripheral interaction model among various quantities in the c.m. system, and the interesting fact is that the matrix element, except for the factor $\sin^2\delta_{33}/q$, has a peak in the high momentum side, which corresponds to low 4-momentum transfer at a certain fixed angle. This behavior is different from the phase

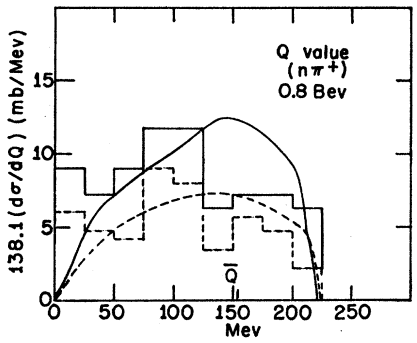

FIG. 13. Q-value distribution of $n\pi^+$ pair at 0.8 Bev.

volume argument. Thus it is expected that decisive differences between our calculations and those of Lindenbaum-Sternheimer will appear in the shape, and the value of the momentum at the maximum will be shifted between the two calculations, unless in their model a forward preference for isobar production is assumed; namely, in their treatment the change of the isobar production angular distribution at high energies from isotropic to a forward preference might correspond to the evidence for the peripheral interaction model.

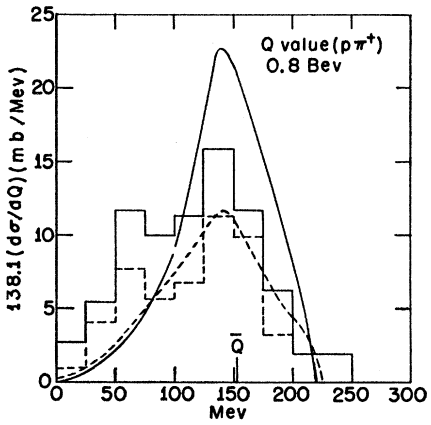

FIG. 14. Q-value distribution of $p\pi^+$ pair at 0.8 Bev.

This point has also been discussed by Chadwick *et al.*[23] in connection with the recoil proton spectrum. Figure 19 shows the result with the normalization of 138.1 times the actual value. We shall report, in future work, on this quantity as well as the other observable quantities in detail.

IV. CONCLUDING REMARKS AND SUMMARY

In this work, we have studied single pion production by nucleon-nucleon collision by means of the picture due to Weiszäcker-Williams and the $(\frac{3}{2},\frac{3}{2})$ resonance approximation. In the course of the study we have made several approximations, for which we gave plausibility arguments. In particular we have made the energy shell approximation for the virtual-pion scattering part. As another possible approximation we might use the off-the-energy shell form of the Chew-Low static meson theory. But this is not suitable in our case. Let us take this approximation and consider the cross section

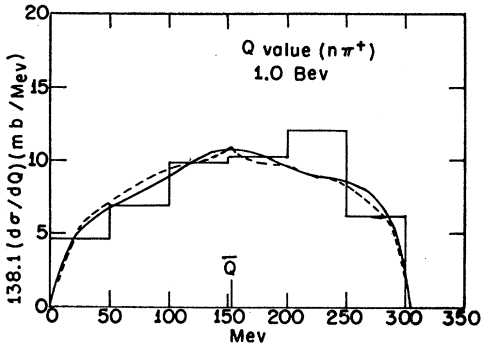

FIG. 15. Q-value distribution of $n\pi^+$ pair at 1.0 Bev.

$\sigma_0(a)$ designating the quantity corresponding to $\sigma(a)$ of the previous approximation. Then we have the difference

$$\sigma_0(a)-\sigma(a)=\Delta\sigma$$
$$=\frac{g^2}{2\pi^2}\frac{1}{p_c W_c}\int\frac{d^3p_2'}{p_{20}'}\frac{t^2}{(t^2+1)^2}\left(\frac{W}{q}\right)\sin^2\delta_{33}$$
$$\times\left[\frac{(t^2+1)(2W^2+2M^2+t^2-1)}{((W+M)^2-1)((W-M)^2-1)}\right]. \quad (22)$$

Thus the integral of $\Delta\sigma$ is equal to that of $\sigma(a)$ except for the last factor in bracket. Since we have the relation

$$\frac{(t^2+1)[2W^2+2M^2+t^2-1]}{[(W+M)^2-1][(W-M)^2-1]}>\frac{t^2+1}{(W-M)^2-1}, \quad (23)$$

Eqs. (22) and (23) mean that (i) $\Delta\sigma$ is positive, (ii) t^2 can easily be larger than a few M, (iii) the

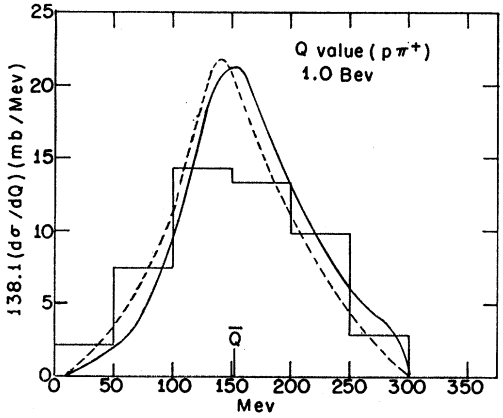

FIG. 16. Q-value distribution of $p\pi^+$ pair at 1.0 Bev.

[23] G. B. Chadwick *et al.*, Phys. Rev. Letters 4, 611 (1960).

interval of integration in the above equations, for which $t^2>$a few M, becomes larger in the Bev energy region, (iv) the rest of the matrix element is dominantly large at $W=\overline{W}$, where $\overline{W}$ is the total energy of the pion-nucleon system at resonance. From these considerations, we reach the conclusion that $\Delta\sigma$ is of the order of or larger than $\sigma(a)$.

For $\sigma(b)$, the inclusion of the factor tt_e/q^2 in Eq. (12) does not have much effect compared to the case of $\sigma(a)$, partly because this inclusion gives a smaller effect than the factor $(t/q)^2$, which is the corresponding factor in $\sigma_0(a)$, and partly because the rest of matrix element in $\sigma(b)$ is quite small as we have mentioned in the preceding section. Thus we reach the conclusion that

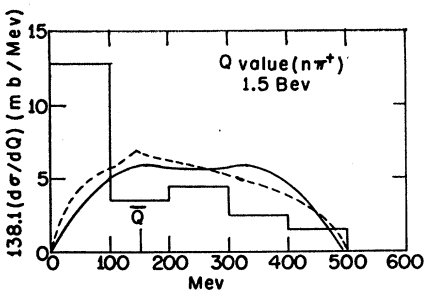

FIG. 17. Q-value distribution of $n\pi^+$ pair at 1.5 Bev.

the off-the-energy shell form of the Chew-Low theory would give a much larger cross section than the energy shell approximation. Since we have found reasonable agreement between our theoretical results and the experimental data, we can rule out the presently considered approximation as untenable.

Next comparisons between our theory and the phenomenological treatment of Lindenbaum and Sternheimer were made in the preceding section, and we found good agreement between the two calculations, though we mentioned slight differences in shapes of the momentum and Q-value distributions. Furthermore, we saw the reason for the change of the assumption made concerning the isobar production angular distribution at high energy as evidence for the peripheral interaction model.

Finally we gave the result of the neutron recoil spectrum, for which the above phenomenological model may give a different result from ours.

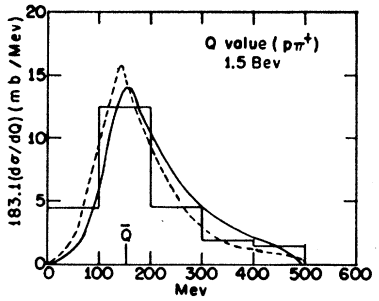

FIG. 18. Q-value distribution of $p\pi^+$ pair at 1.5 Bev.

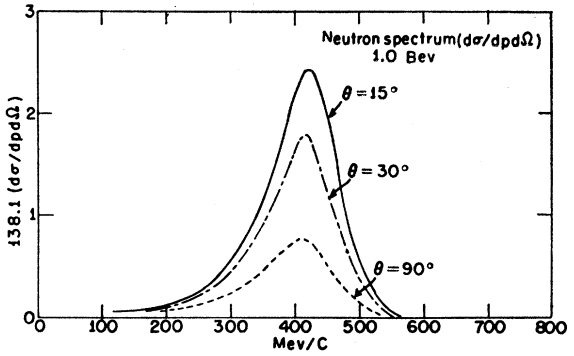

FIG. 19. Neutron recoil spectrum, $d\sigma(p,\Omega)/dpd\Omega$, at 1.0 Bev, as predicted by the theory of this paper.

APPENDIX

To obtain Eq. (18) from Eq. (12) we make the following approximations. Let us consider

$$I=\int\delta^4(p_1'+p_2'+q-p_1-p_2)\frac{d^3p_2'}{p_{20}'}\frac{d^3q}{q_0}\frac{t^2}{(t^2+1)^2}(3x^2+1),$$

$$=\frac{p_2'^2dp_2'}{p_{20}'}\frac{1}{2p_1'p_2'}\int d\varphi\frac{t^2}{(t^2+1)^2}(3x^2+1),$$

$$x=\hat{q}\cdot\hat{t},$$

where we take the coordinate system shown in Fig. 20.

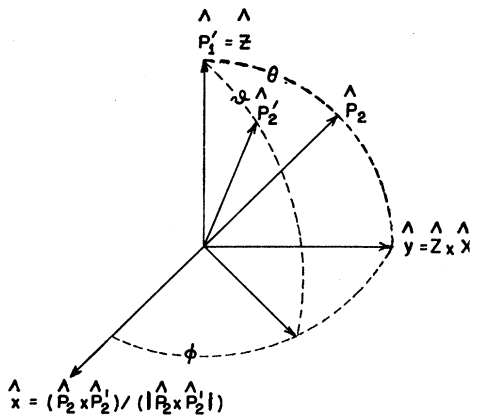

FIG. 20. The coordinate system for the integral I.

The integrand of the second equation is a very complex function of $\sin\varphi$. Therefore we neglect φ dependence in the integrand and also make the approximation $3x^2+1\rightarrow\langle 3x^2+1\rangle=2$. Then we have

$$t^2+1\approx W_cp_{20}'+1-2M^2-2p_cp_2'\cos\vartheta\cos\theta,$$

$$\cos\vartheta=[(W_c-p_{10}'-p_{20}')^2-p_1'^2-p_2'^2-1]/2p_1'p_2'.$$

The integral range of p_2' can then be obtained by the condition $|\cos\vartheta|\leqslant 1$.